Chapter 22

Off-Axis imaging: comparing HSI images to raytrace models

Terrance J. Gaetz

A number of off-axis HSI exposures were made in order to explore the off-axis PSF. It was initially planned to take full HRMA exposures at $10'$ and $20'$ (pure *yaw*), and at $5'$, $15'$, $25'$, and $30'$ ($pitch = -yaw$); they were to be taken at four energies, C-Kα (0.277 keV), Al-Kα (1.486 keV), Ti-Kα (4.51 keV), and Fe-Kα (6.4 keV). The initial exposures (C-Kα) showed structure which supported the speculation that the observed imbalances in the flux balance tests were due to an internal Parabola to Hyperbola decenter error. Further off-axis images, together with raytrace analysis, indicated that at least two shells had decenter errors. It was decided to replace the planned set of full HRMA exposures with a set of single-shell exposures; in order to provide more coverage of the off-axis direction, the $30'$ single shell exposures were taken with $pitch \simeq yaw$ rather than $pitch = -yaw$ as was done for the other energies. Analysis of these images, together with raytrace simulations of the effects of mirror misalignments, allowed a set of rigid-body decenters (plus compensating tilts) to be derived; this is discussed more fully in Chapter 30.

In this chapter the high fidelity raytrace model is used to compare raytraced images (based on the derived rigid-body parameter sets) with the HSI off-axis images obtained at XRCF. The raytrace images include the effects of the HSI angle-dependent relative quantum efficiency.

In Table 22.1, the off-axis HSI images are listed.

22.1 Off-axis HSI Images (Full HRMA)

the 25 and $30'$ off-axis images show ghost images. The positions and shapes of the ghosts are very sensitive to off-axis angle; the pitch and yaw need to be tweaked to get better agreement for the ghosts.

Table 22.1: Phase 1 Off-Axis Images (Full HRMA)

TRW ID	RunID	Energy	Shell	pitch	yaw	defocus	Counts
E-IXH-PI-6.001	110594	0.277	HRMA	−3.54	3.54	1.4384	103775
E-IXH-PI-7.002	110639	0.277	HRMA	0	−10	5.6211	103208
E-IXH-PI-6.003	110668	0.277	HRMA	−10.61	10.61	12.1095	100412
E-IXH-PI-7.004	110669	0.277	HRMA	0	−20	20.6847	73019
E-IXH-PI-6.005	110700	0.277	HRMA	−17.68	17.68	31.1065	48864
E-IXH-PI-6.006	110701	0.277	HRMA	−21.21	21.21	44.7368	32438
E-IXH-PI-12.004	110887	6.4	HRMA	0	−20	20.6847	81715
E-IXH-PI-12.002	110888	6.4	HRMA	0	−10	5.6211	98095
E-IXH-PI-11.001	110889	6.4	HRMA	−3.54	3.54	1.4384	93828
E-IXH-PI-11.003	110890	6.4	HRMA	−10.61	10.61	12.1095	96178
E-IXH-PI-11.005	110892	6.4	HRMA	−17.68	17.68	31.1065	128426
E-IXH-PI-11.006	110893	6.4	HRMA	−21.21	21.21	44.7368	282273
E-IXH-PI-22.004	111084	4.51	HRMA	0	−20	20.6847	74416
E-IXH-PI-22.002	111085	4.51	HRMA	0	−10	5.6211	103047
E-IXH-PI-21.001	111086	4.51	HRMA	−3.54	3.54	1.4384	99238
E-IXH-PI-21.003	111087	4.51	HRMA	−10.61	10.61	12.1095	98197
E-IXH-PI-21.005	111088	4.51	HRMA	−17.68	17.68	31.1065	56639
E-IXH-PI-21.006	111089	4.51	HRMA	−21.21	21.21	44.7368	58039
E-IXH-PI-50.001	111757	1.486	6	0	−20	54.1046	90934
E-IXH-PI-50.002	111758	1.486	4	0	−20	30.2079	80047
E-IXH-PI-50.003	111759	1.486	3	0	−20	23.6882	58430
E-IXH-PI-50.004	111760	1.486	1	0	−20	15.5253	84628
E-IXH-PI-51.001	111761	1.486	6	−10.61	10.61	30.3917	87750
E-IXH-PI-51.002	111762	1.486	4	−10.61	10.61	17.4109	86283
E-IXH-PI-51.003	111763	1.486	3	−10.61	10.61	13.6771	85855
E-IXH-PI-51.004	111764	1.486	1	−10.61	10.61	9.0284	86542
E-IXH-PI-52.001	111765	1.486	6	16.42	17.68	85.0136	98126
E-IXH-PI-52.002	111766	1.486	4	16.42	17.68	46.4008	75388
E-IXH-PI-52.003	111767	1.486	3	16.42	17.68	36.0489	67708
E-IXH-PI-52.004	111768	1.486	1	16.42	17.68	23.6816	75210

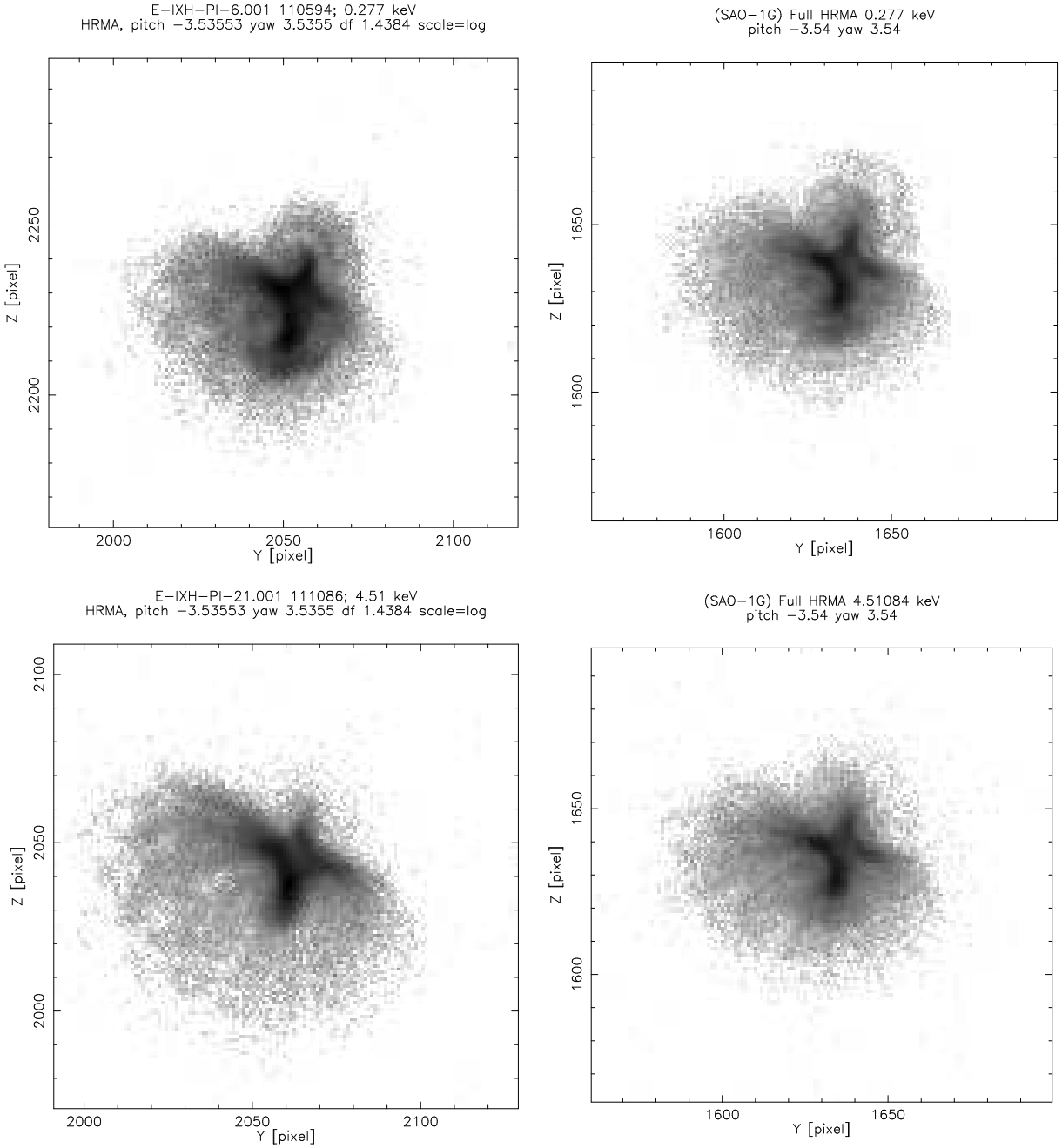

Figure 22.1: Top left: hsi110594i0 X-ray image; 5′ off-axis, C-Kα. (1×1 HSI pixel.) Top right: Raytrace; 5′ off-axis, C-Kα. (1×1 HSI pixel.) Bottom left: hsi111086i0 X-ray image; 5′ off-axis, Ti-Kα. (1×1 HSI pixel.) Bottom right: Raytrace; 5′ off-axis, Ti-Kα. (1×1 HSI pixel.) The images are log stretched.

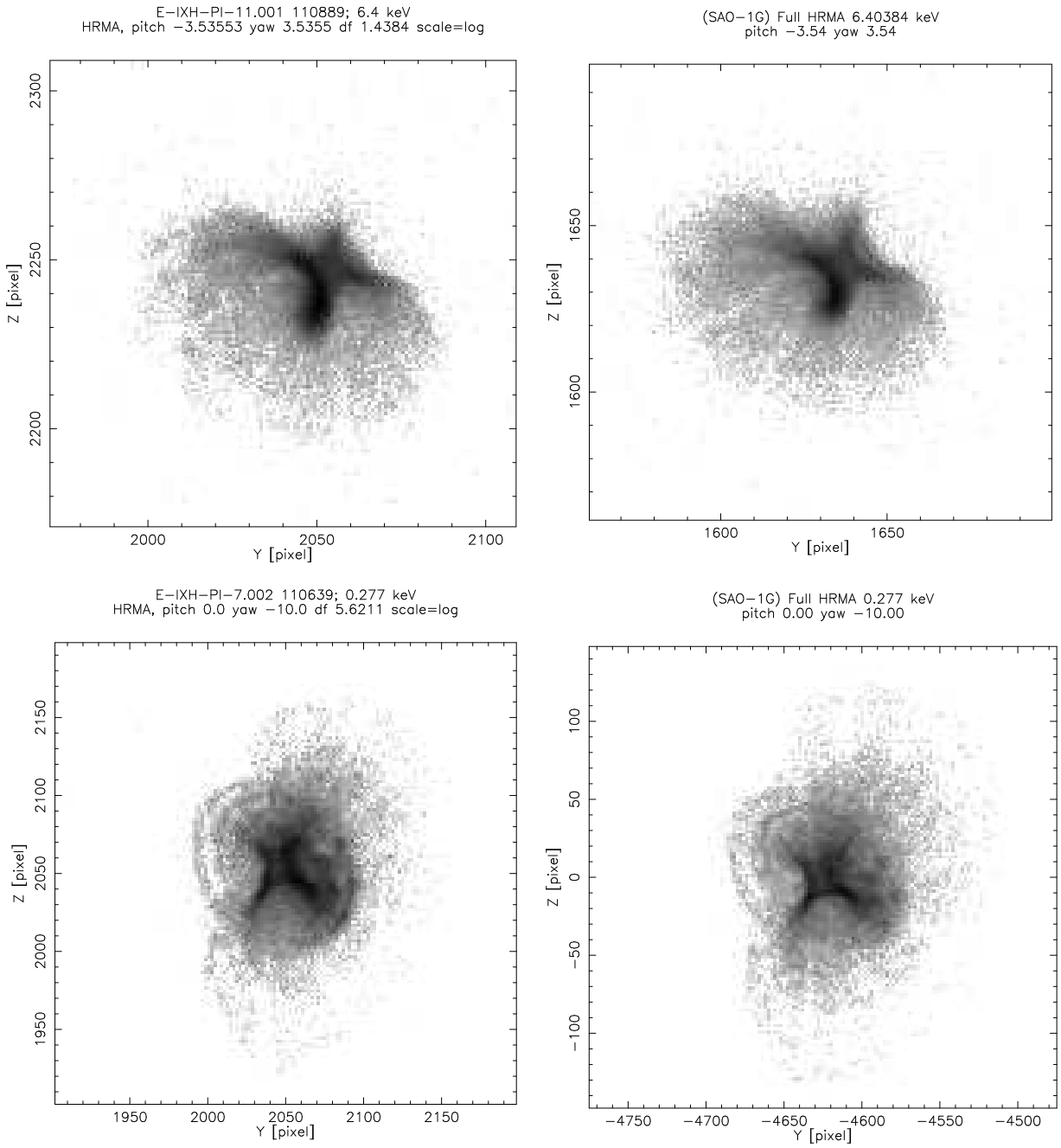

Figure 22.2: Top left: hsi110889i0 X-ray image; 5′ off-axis, Fe-Kα. (1×1 HSI pixel.) Top right: Raytrace; 5′ off-axis, Fe-Kα. (1×1 HSI pixel.) Bottom left: hsi111086i0 X-ray image; 10′ off-axis, C-Kα. (2×2 HSI pixels.) Bottom right: Raytrace; 10′ off-axis, C-Kα. (2×2 HSI pixels.) The images are log stretched.

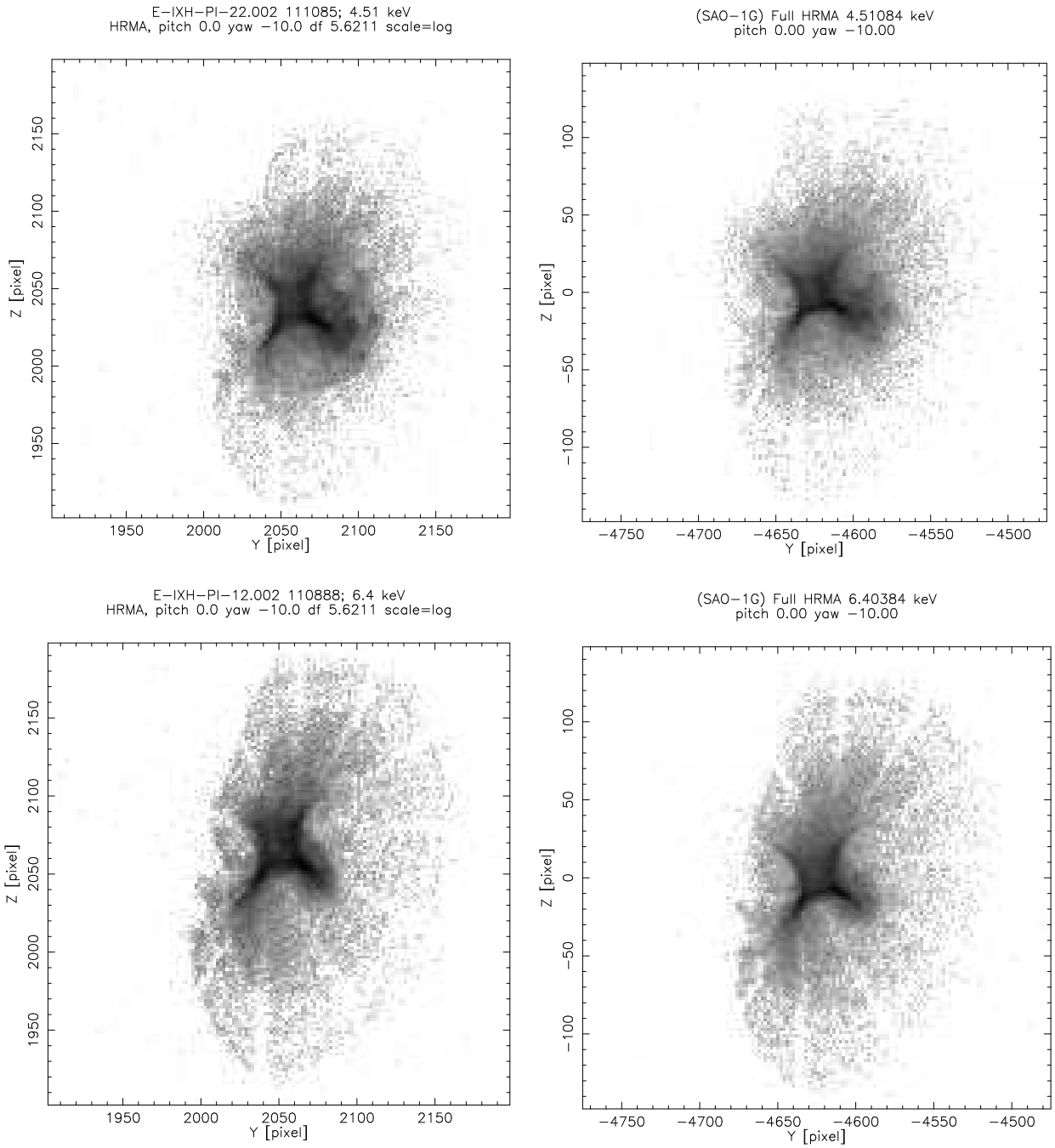

Figure 22.3: Top left: hsi111085i0 X-ray image; 10′ off-axis, Ti-Kα. (2×2 HSI pixels.) Top right: Raytrace; 10′ off-axis, Ti-Kα. (2×2 HSI pixels.) Bottom left: hsi110888i0 X-ray image; 10′ off-axis, Fe-Kα. (2×2 HSI pixels.) Bottom right: Raytrace; 10′ off-axis, Fe-Kα. (2×2 HSI pixels.) The images are log stretched.

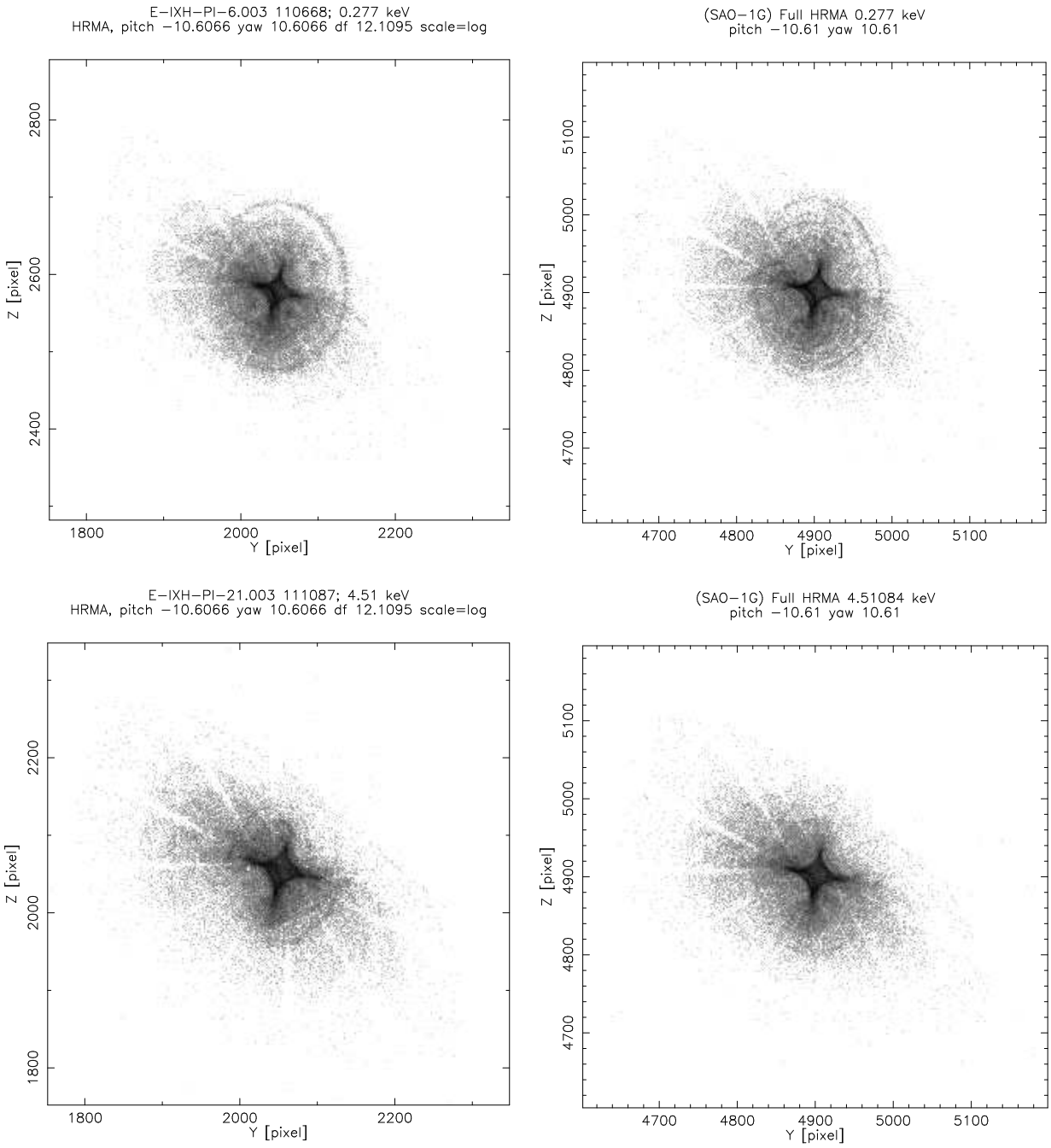

Figure 22.4: Top left: hsi110668i0 X-ray image; 15′ off-axis, C-Kα. (2×2 HSI pixels.) Top right: Raytrace; 15′ off-axis, C-Kα. (2×2 HSI pixels.) Bottom left: hsi111087i0 X-ray image; 15′ off-axis, Ti-Kα. (2×2 HSI pixels.) Bottom right: Raytrace; 15′ off-axis, Ti-Kα. (2×2 HSI pixels.) The images are log stretched.

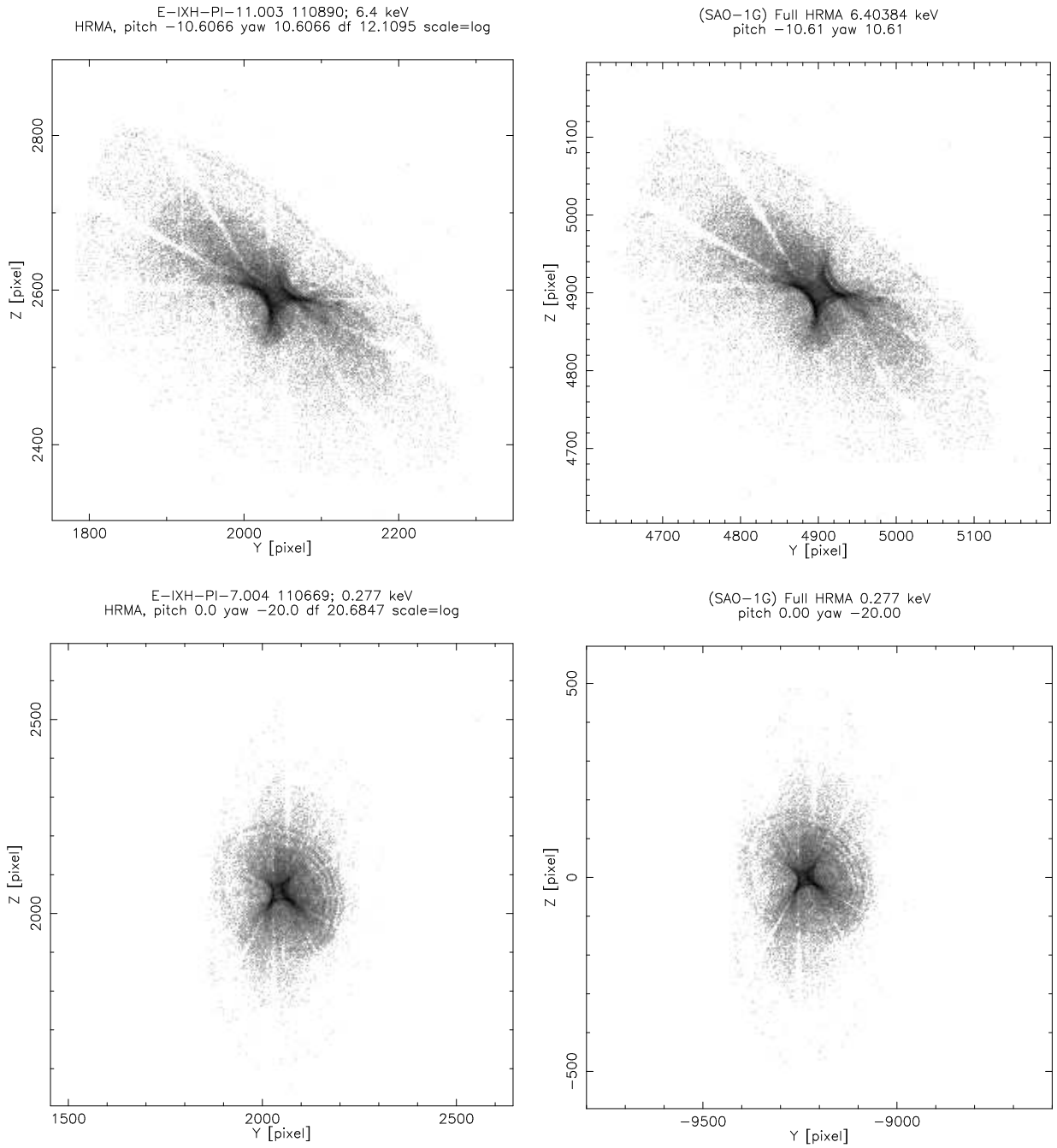

Figure 22.5: Top left: hsi110890i0 X-ray image; 15′ off-axis, Fe-Kα. (4×4 HSI pixels.) Top right: Raytrace; 15′ off-axis, Fe-Kα. (4×4 HSI pixels.) Bottom left: hsi110669i0 X-ray image; 20′ off-axis, C-Kα. (4×4 HSI pixels.) Bottom right: Raytrace; 20′ off-axis, C-Kα. (4×4 HSI pixels.) The images are log stretched.

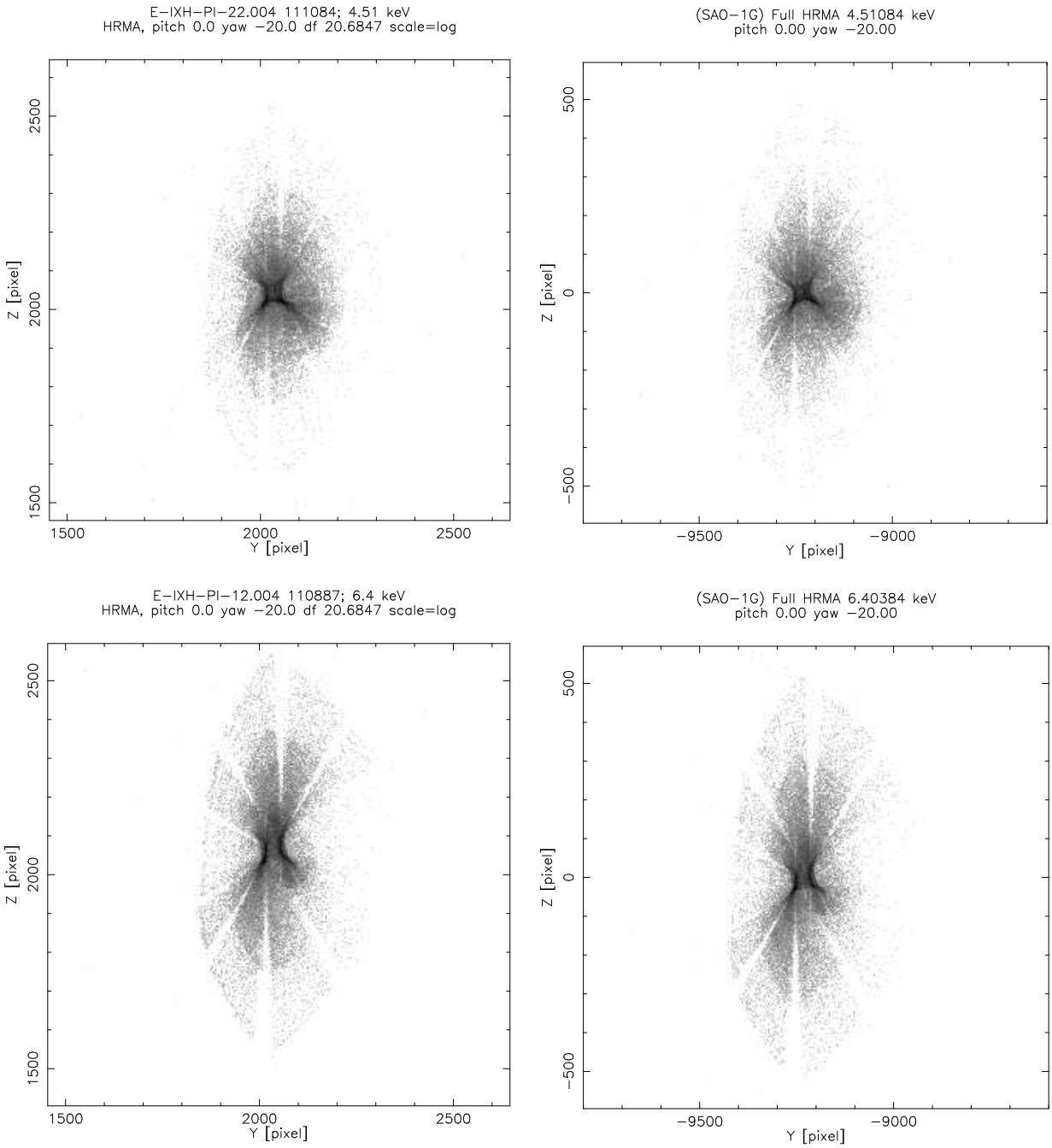

Figure 22.6: Top left: hsi111084i0 X-ray image; 20′ off-axis, Ti-Kα. (4×4 HSI pixels.) Top right: Raytrace; 20′ off-axis, Ti-Kα. (4×4 HSI pixels.) Bottom left: hsi110887i0 X-ray image; 20′ off-axis, Fe-Kα. (4×4 HSI pixels.) Bottom right: Raytrace; 20′ off-axis, Fe-Kα. (4×4 HSI pixels.) The images are log stretched.

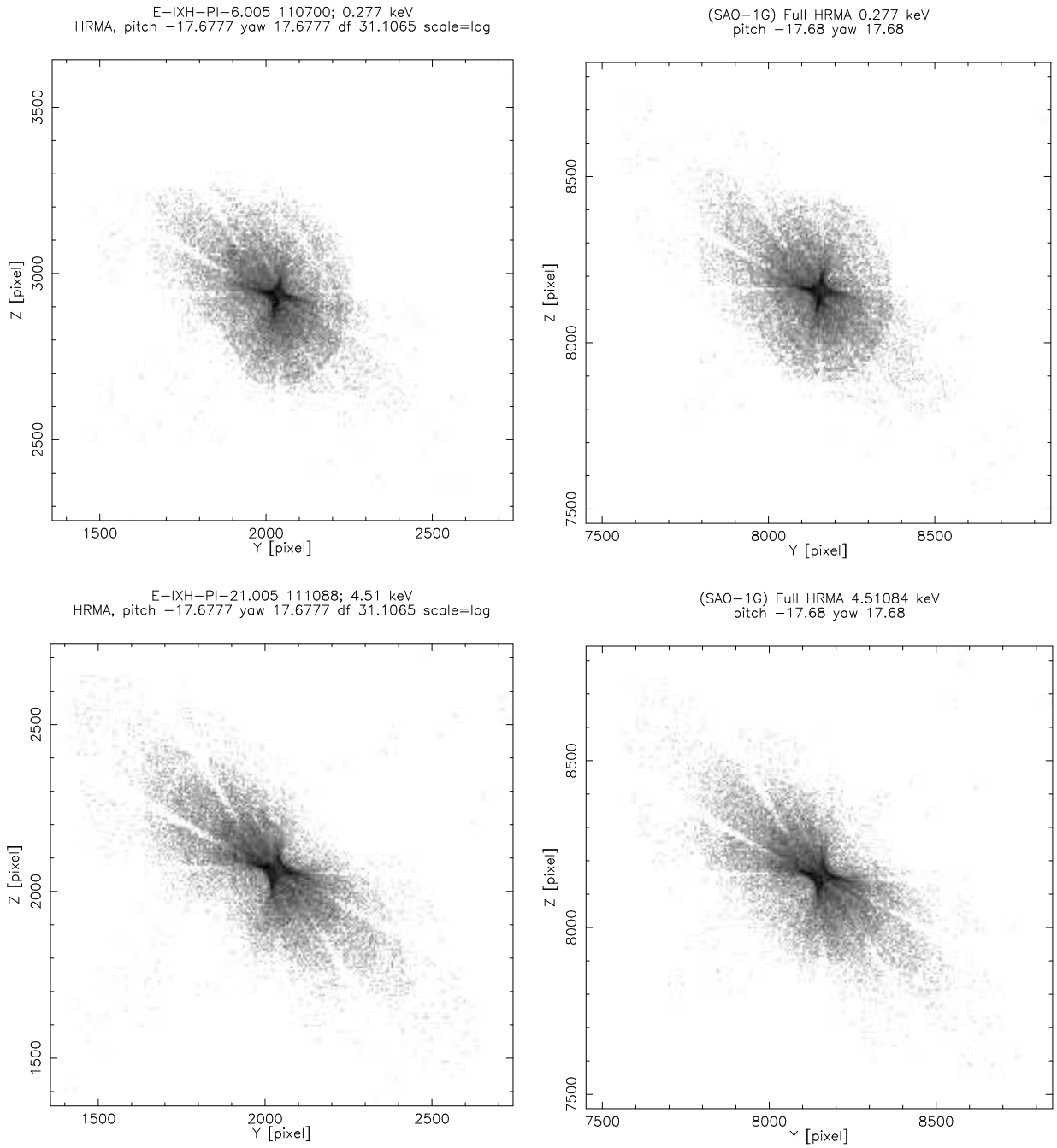

Figure 22.7: Top left: hsi110700i0 X-ray image; 25′ off-axis, C-Kα. (6×6 HSI pixels.) Top right: Raytrace; 25′ off-axis, C-Kα. (6×6 HSI pixels.) Bottom left: hsi111088i0 X-ray image; 25′ off-axis, Ti-Kα. (6×6 HSI pixels.) Bottom right: Raytrace; 25′ off-axis, Ti-Kα. (6×6 HSI pixels.) The images are log stretched.

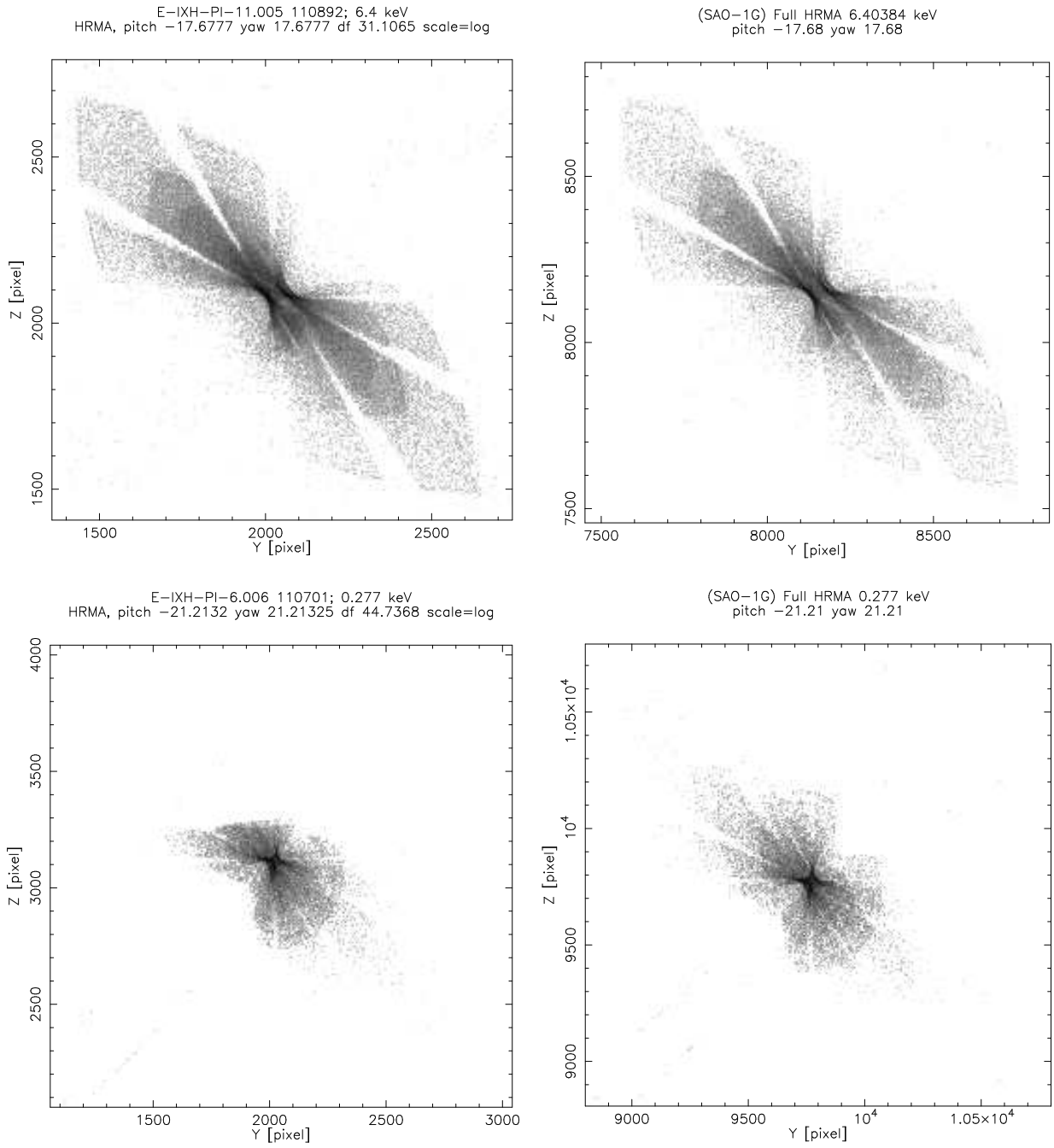

Figure 22.8: Top left: hsi110892i0 X-ray image; 25′ off-axis, Fe-Kα. (6×6 HSI pixels.) Top right: Raytrace; 25′ off-axis, Fe-Kα. (6×6 HSI pixels.) Bottom left: hsi110701i0 X-ray image; 30′ off-axis, C-Kα. (8×8 HSI pixels.) Bottom right: Raytrace; 30′ off-axis, C-Kα. (8×8 HSI pixels.) The images are log stretched. The C-Kα 35′ image was taken near the edge of the HSI detector; this caused part of the image to fall off the detector.

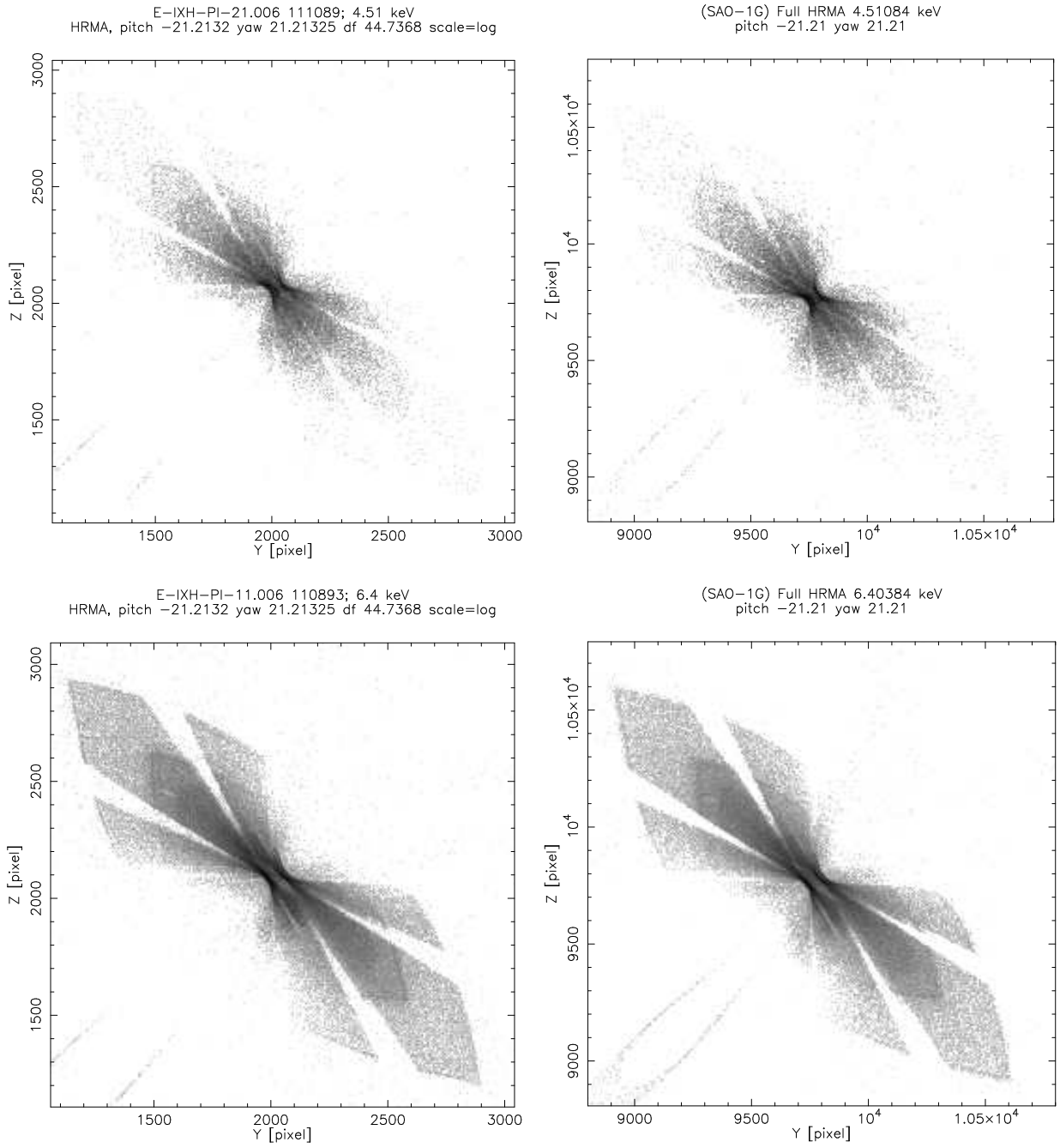

Figure 22.9: Top left: hsi111089i0 X-ray image; 30′ off-axis, Ti-Kα. (8×8 HSI pixels.) Top right: Raytrace; 30′ off-axis, Ti-Kα. (8×8 HSI pixels.) Bottom left: hsi110893i0 X-ray image; 30′ off-axis, Fe-Kα. (8×8 HSI pixels.) Bottom right: Raytrace; 30′ off-axis, Fe-Kα. (8×8 HSI pixels.) The images are log stretched.

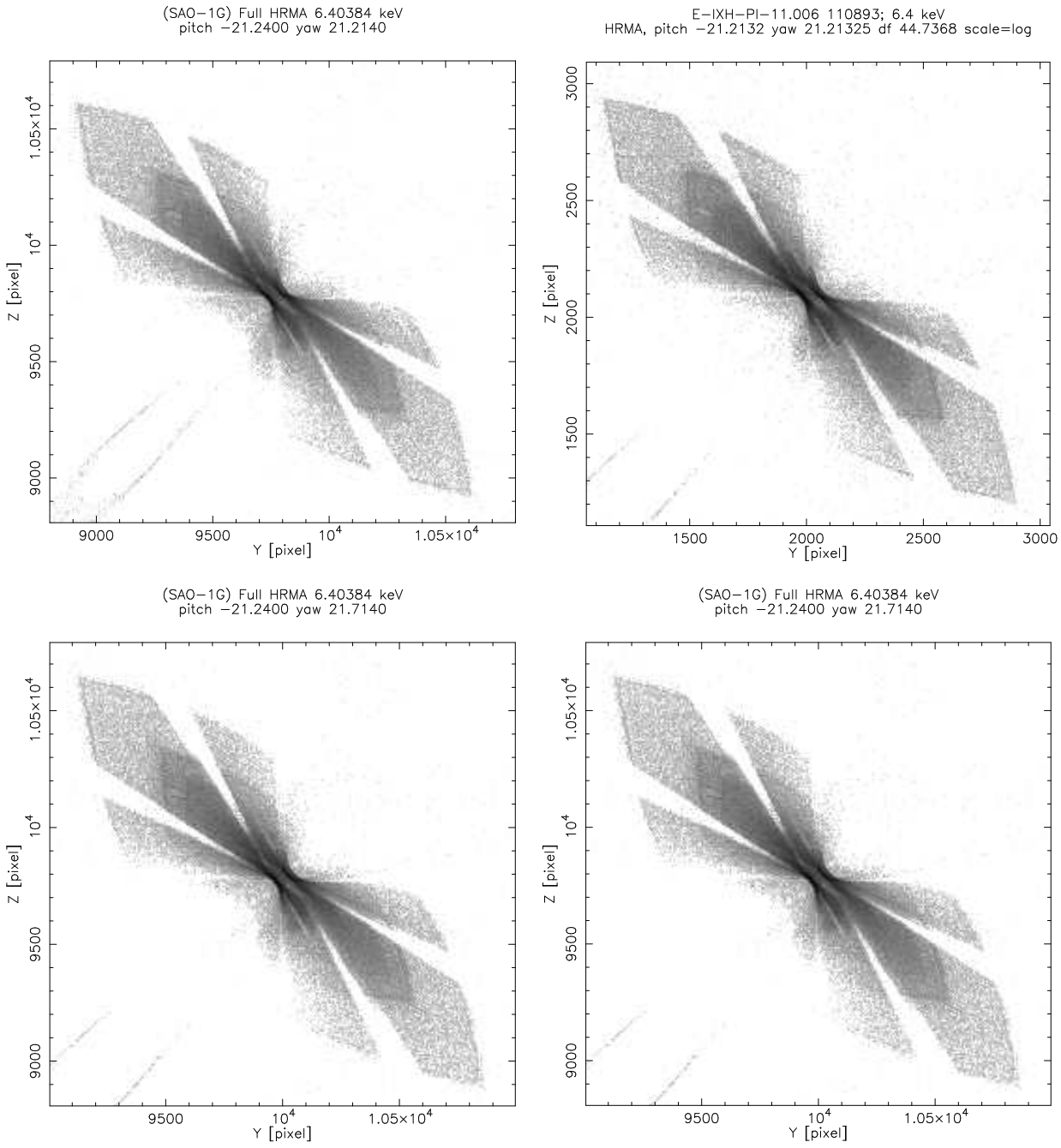

Figure 22.10: Top left: Raytrace; nominal IAP setting. (8×8 HSI pixels.) Top right: hsi110893i0 X-ray image; 30′ off-axis, Fe-Kα. (8×8 HSI pixels.) Bottom left: Raytrace; nominal IAP + 0.5 arcmin yaw. (8×8 HSI pixels.) Bottom right: Raytrace; nominal IAP + 0.5 arcmin yaw. (8×8 HSI pixels.) The images are log stretched.

22.2 Off-axis HSI Images (Single Shell)

In order to better diagnose the coma-free decenters, a planned set of full-HRMA off-axis images at Al-Kα was replaced by a set of single shell images at Al-Kα. These were used to diagnose the magnitude and direction of the decenters (see Chapter 30).

In addition, it is apparent that the quadrant shutters are vignetting the single shell images. This is particularly noticeable in the 20 and $25'$ off-axis single shell images. These can be used to refine the knowledge of misalignment of the quadrant shutter assembly. **Work in progress; to be done: raytraces with the misaligned quadrant shutters.**

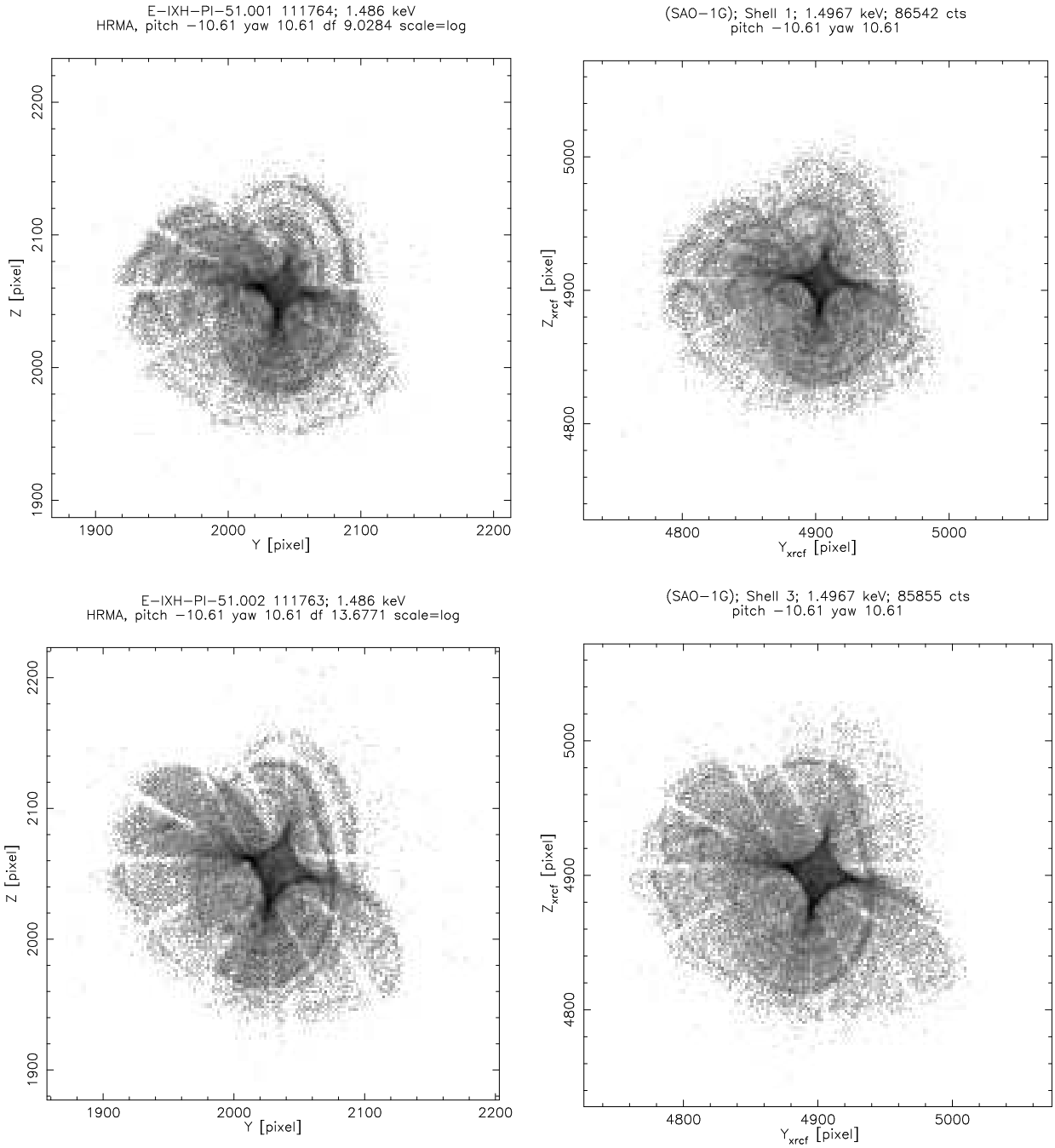

Figure 22.11: Top left: hsi111764i0 X-ray image; shell 1, 15′ off-axis, Al-Kα. (2×2 HSI pixels.) Top right: Raytrace; shell 1, 15′ off-axis, Al-Kα. (2×2 HSI pixels.) Bottom left: hsi111763i0 X-ray image; shell 3, 15′ off-axis, Al-Kα. (2×2 HSI pixels.) Bottom right: Raytrace; shell 3, 15′ off-axis, Al-Kα. (2×2 HSI pixels.) The images are log stretched.

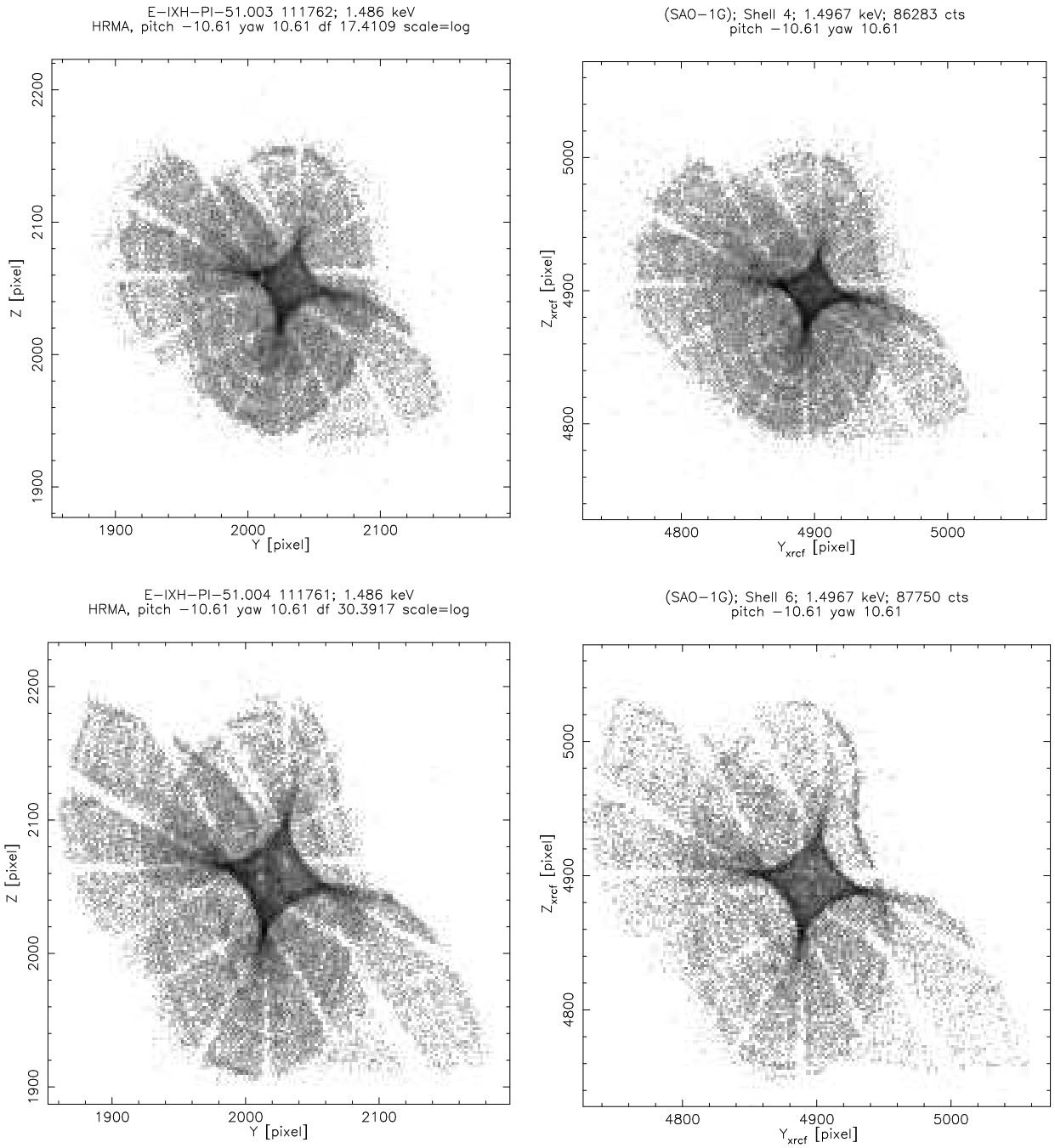

Figure 22.12: Top left: hsi111762i0 X-ray image; shell 4, 15′ off-axis, Al-Kα. (2×2 HSI pixels.) Top right: Raytrace; shell 4, 15′ off-axis, Al-Kα. (2×2 HSI pixels.) Bottom left: hsi111761i0 X-ray image; shell 6, 15′ off-axis, Al-Kα. (2×2 HSI pixels.) Bottom right: Raytrace; shell 6, 15′ off-axis, Al-Kα. (2×2 HSI pixels.) The images are log stretched.

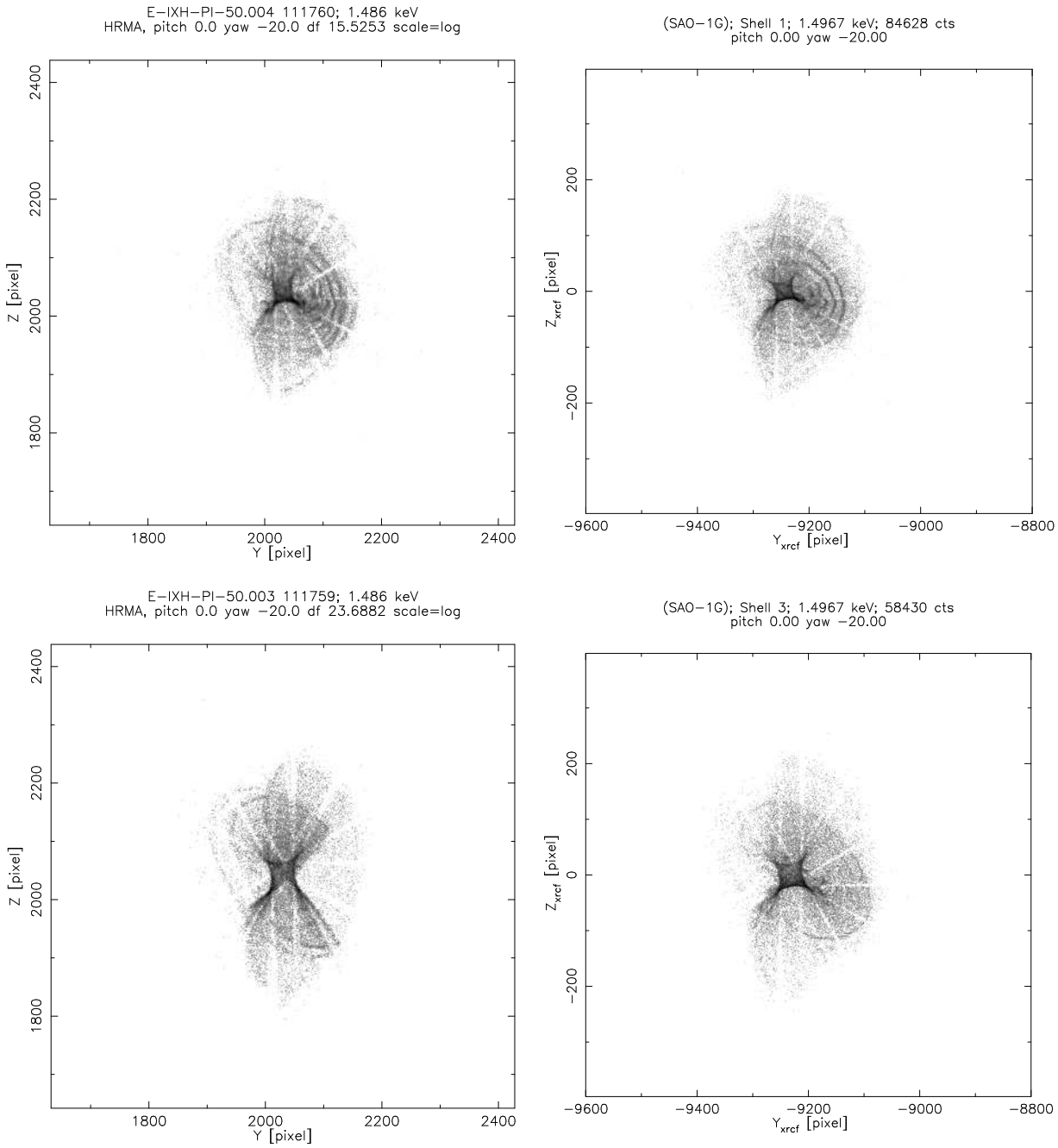

Figure 22.13: Top left: hsi111760i0 X-ray image; shell 1, 20′ off-axis, Al-Kα. (2×2 HSI pixels.) Top right: Raytrace; shell 1, 20′ off-axis, Al-Kα. (2×2 HSI pixels.) Bottom left: hsi111759i0 X-ray image; shell 3, 20′ off-axis, Al-Kα. (2×2 HSI pixels.) Bottom right: Raytrace; shell 3, 20′ off-axis, Al-Kα. (2×2 HSI pixels.) The images are log stretched.

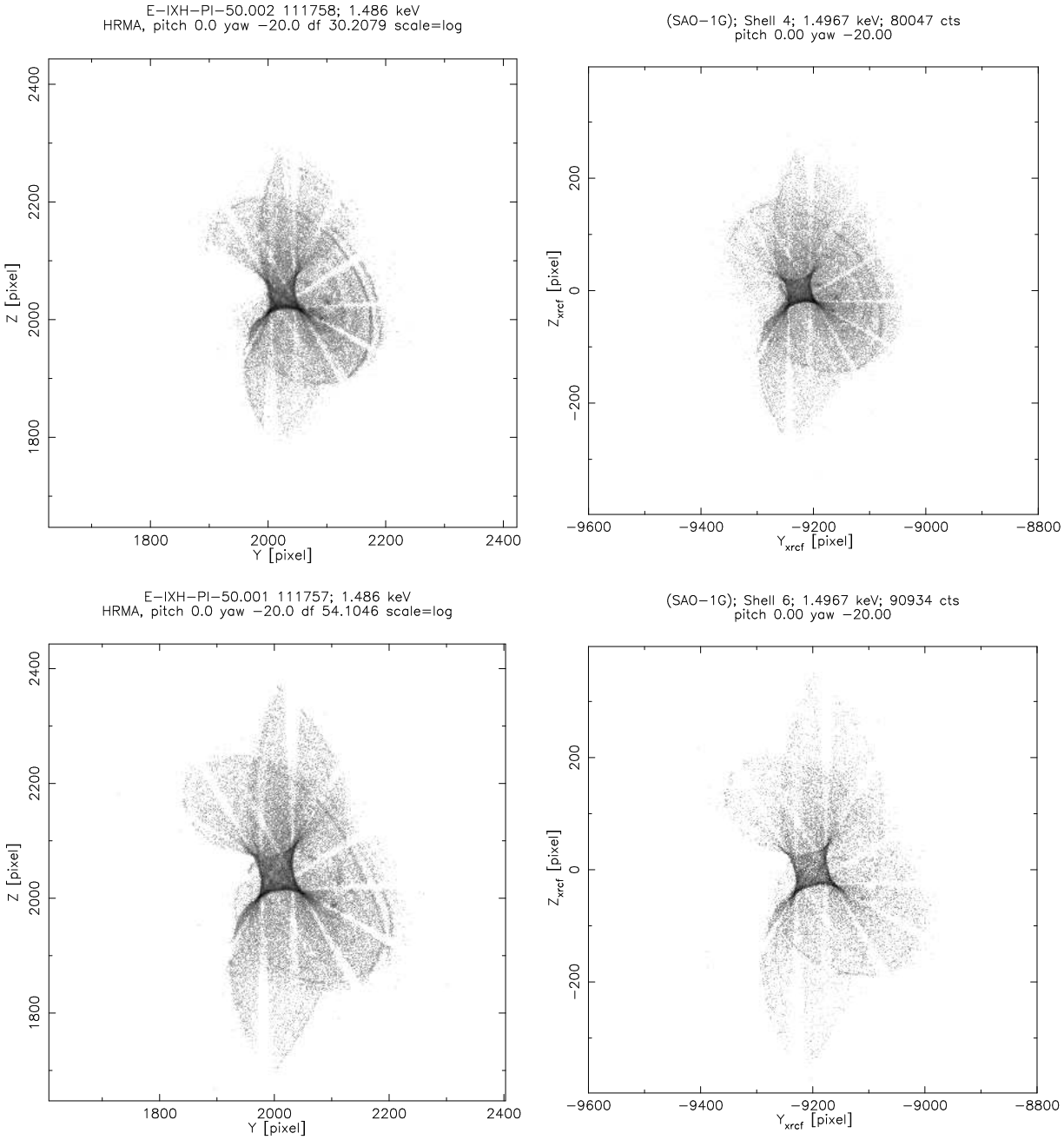

Figure 22.14: Top left: hsi111758i0 X-ray image; shell 4, 20′ off-axis, Al-Kα. (2×2 HSI pixels.) Top right: Raytrace; shell 4, 20′ off-axis, Al-Kα. (2×2 HSI pixels.) Bottom left: hsi111757i0 X-ray image; shell 6, 20′ off-axis, Al-Kα. (2×2 HSI pixels.) Bottom right: Raytrace; shell 6, 20′ off-axis, Al-Kα. (2×2 HSI pixels.) The images are log stretched.

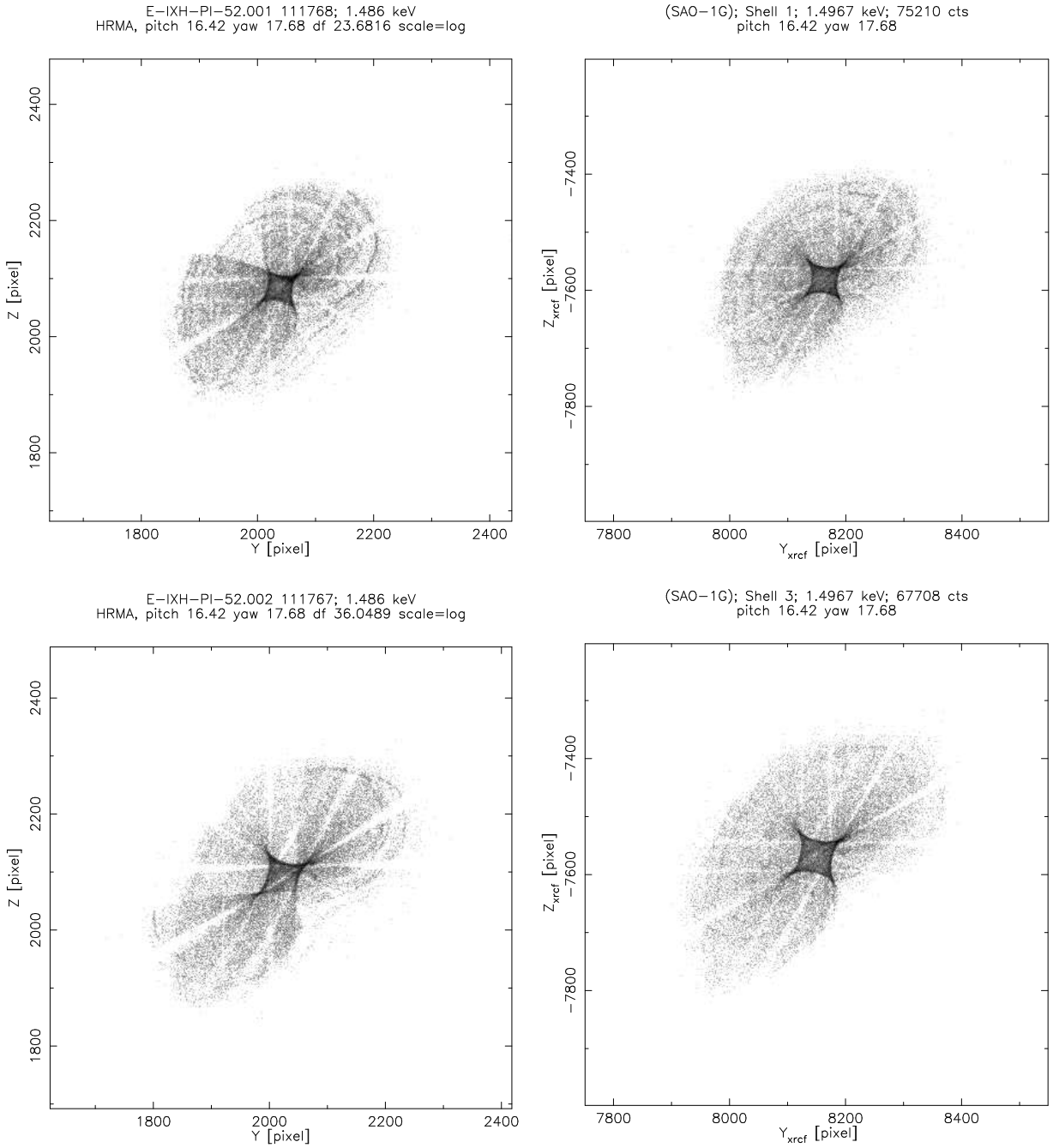

Figure 22.15: Top left: hsi111768i0 X-ray image; shell 1, 24′ off-axis, Al-Kα. (2×2 HSI pixels.) Top right: Raytrace; shell 1, 24′ off-axis, Al-Kα. (2×2 HSI pixels.) Bottom left: hsi111767i0 X-ray image; shell 3, 24′ off-axis, Al-Kα. (2×2 HSI pixels.) Bottom right: Raytrace; shell 3, 24′ off-axis, Al-Kα. (2×2 HSI pixels.) The images are log stretched.

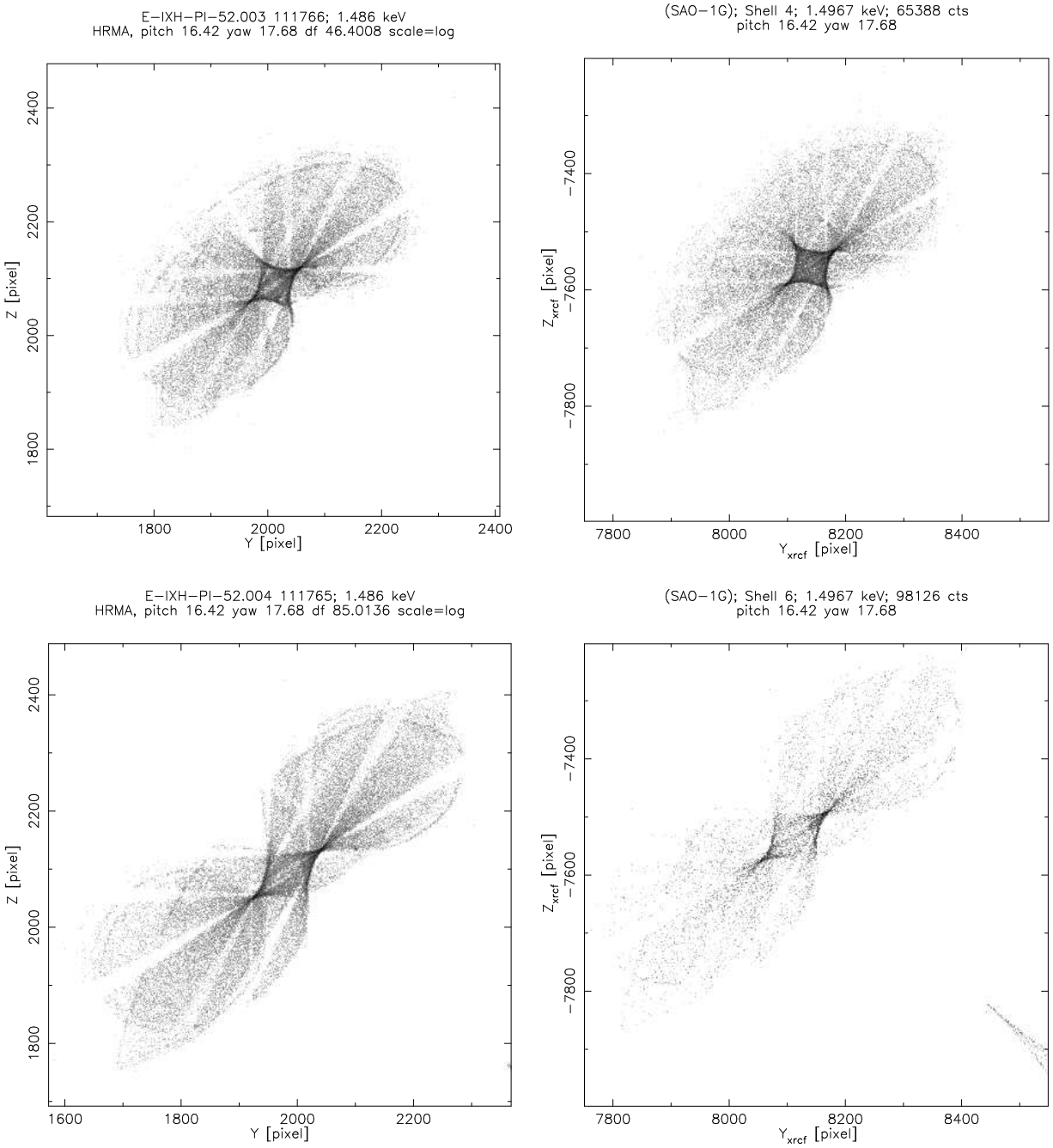

Figure 22.16: Top left: hsi111766i0 X-ray image; shell 4, 24′ off-axis, Al-Kα. (2×2 HSI pixels.) Top right: Raytrace; shell 4, 24′ off-axis, Al-Kα. (2×2 HSI pixels.) Bottom left: hsi111765i0 X-ray image; shell 6, 24′ off-axis, Al-Kα. (2×2 HSI pixels.) Bottom right: Raytrace; shell 6, 24′ off-axis, Al-Kα. (2×2 HSI pixels.) The images are log stretched.